

A THREE-DIMENSIONAL MODEL FOR RAIN-WIND INDUCED VIBRATION OF STAY CABLES IN CABLE-STAYED BRIDGES

Truong Viet Hung^{a,*}, Vu Quang Viet^b, Vu Quoc Anh^c

^a*Faculty of Civil Engineering, Thuyloi University, 175 Tay Son street, Dong Da district, Hanoi, Vietnam*

^b*Faculty of Civil Engineering, Vietnam Maritime University, 484 Lach Tray street, Le Chan district, Hai Phong city, Vietnam*

^c*Faculty of Civil Engineering, Hanoi Architectural University, Nguyen Trai road, Hanoi, Vietnam*

Article history:

Received 02/07/2019, Revised 12/08/2019, Accepted 12/08/2019

Abstract

In this paper, the effects of wind velocity according to height above the ground on the rain-wind induced vibration (RWIV) of stay cables are investigated. RWIV of the cable is modeled using the linear theory of cable vibration and the central difference algorithm. The wind speed profile according to height above the ground, which affects both aerodynamic forces acting on the cable and the oscillation of the rivulet on the cable surface, is taken into account in the theoretical formulation. The fourth-order method Runge-Kutta is used for solving the system of differential equation of the cable oscillation. The proposed 3D model of the stay cable is then used to assess the effects of wind velocity distribution on cable RWIV. The results obtained in this study showed that in most current cable-stayed bridges, in which the height of pylons is lower than 200 m, the change of wind velocity according to the height above the ground should be included in RWIV analyses.

Keywords: stay cable; rain - wind induced vibration; rivulet; analytical model; vibration.

[https://doi.org/10.31814/stce.nuce2020-14\(1\)-08](https://doi.org/10.31814/stce.nuce2020-14(1)-08) © 2020 National University of Civil Engineering

1. Introduction

Owing to the rapid development of construction technologies and new advanced materials, more and more bridges with super long-span and slimmer shape have been built throughout the world. However, the longer and slimmer the bridges are, the more difficulties we have to face in analysis and design, especially aerodynamic effects such as buffeting, vortex, flutter and turbulence (refers Refs. [1–4], among others). In among many components of a cable-stayed bridge, stay cables with a very long length and a small cross-sectional area have low damping factors and a wide range of natural frequencies. Hence, they are very sensitive with aerodynamic effects. Rain-wind induced vibration (RWIV), first observed by Hikami and Shiraishi [5], is one of the critical aerodynamic phenomena of stay cables that has a significant attention of researchers.

RWIV is a large amplitude and low frequency vibration of cables in cable-stayed bridges under the effects of wind and rain [6]. Hikami and Shiraishi mentioned in [5] that this phenomenon might not be explained by using vortex-induced oscillations or a wake galloping because the frequency of

*Corresponding author. *E-mail address:* truongviethung@tlu.edu.vn (Hung, T. V.)

a RWIV vibration is lower than the critical one of the vortex-induced vibrations, and the distances between cables are too large to a wake galloping phenomenon can occur. After the work of Hikami and Shiraishi, a series of laboratory experiments and wind tunnel tests (Matsumoto et al. [7], Flamand [8], Gu and Du [9], Gu [10], Gao et al. [11], Jing et al. [12], Du et al. [13], Jing et al. [14], etc.) were conducted to find the cause of this phenomenon. The results of these studies proved that the formation of the upper rivulet on cable surface under a normal wind speed and low or moderate rainfall, which can oscillate with lower modes, was the basic RWIV characteristic. The vibration amplitude of RWIV was also discovered by Wu et al. [15] to depend on the cable surface material, cable inclination direction, and wind angle. Cosentino et al. [16], Macdonald and Larose [17], Flamand and Boujard [18], Zuo and Jones [19] found out that the RWIV phenomenon is related to Reynolds number effects, and there are some similarities between the mechanisms of the RWIV and the dry galloping phenomenon of cables. Recently, Du et al. [20] discovered that the significant change of aerodynamic forces acting on the cable and the rivulet when the upper rivulet located at different positions may be the excitation mechanics of the RWIV.

To look into the nature of this phenomenon, lots of theoretical models explaining it have been developed. 2D models were first developed to study the behaviors of RWIV of the stay cables such as the two-degree-of-freedom theory (2-DOF) proposed by Yamaguchi [21], the single-degree-of-freedom (SDOF) model developed by Xu and Wang [22], Wilde and Witkowski [23], and Hung and Viet [24]. In the 2D models, the upper rivulet is assumed to have the same frequency with the cable's. When the rivulet oscillates on the cable surface, the relative mean velocity and angle of the wind to the cable are changed continuously. The drag and lift aerodynamic forces therefore are constantly changed. In some specific terms of wind speed and upper rivulet position on the cable surface, the aerodynamic damping is negative that leads to a great amplitude of the cable vibration. In addition, Lemaitre et al. [25] modelled the rivulet formation by using the lubrication theory to investigate the variation of water films around the cables. Thereafter, Bi et al. [26] combined vibration and lubrication theories to develop a 2D coupled equations model of water film evolution and cable oscillation. Jing et al. [27] used the boundary layer state to develop a theoretical 2D cable model. Recently, a 3D model of cable has been used in the investigation of RWIV but the number of studies is still limited. Some interesting works can be listed here are Gu [10], Li et al. [28–30], Liu et al. [31], etc. In all aforementioned studies, the authors considered the wind impacting on the cable with a constant speed. Obviously, this assumption is inconsistent with the fact that wind speed increases with increasing height above the ground. With different wind speed, the unstable balance position of the rivulet on the cable surface is changed. This leads to the change of aerodynamic forces acting on the cable, and then the cable RWIV is not the same with the case where wind speed is constant. Therefore, the results of the above researches may not match the reality.

In this study, the influences of wind velocity according to height above the ground on the RWIV of stay cables are investigated. To achieve this goal, a 3D model for RWIV of stay cables of cable-stayed bridges is developed first using the linear theory of cable vibration [32] and the central difference algorithm. The aerodynamic force functions proposed by Hung and Viet [24] are employed to estimate the aerodynamic forces acting on cable elements. The change of wind velocity, inclination angle of the cable, and the initial position of rivulet according to the cable height, which affect both aerodynamic forces and the rivulet vibration, is taken into account in the theoretical formulation. The developed model of the cable is then used to investigate the influences of the wind velocity distribution according to height above the ground.

2. 3D model for analysis of RWIV of inclined cables

In this section, a 3D model of an inclined cable with two fixed points is developed using the linear theory of cable vibration [32] and the central difference algorithm. The mean wind velocity profile is taken into account in the theoretical formulation. The aerodynamic forces acting on the cable are obtained by using the equations proposed by Hung and Viet [24] but the effects of the cable height are considered since the wind velocities, inclination angle, and the initial position of rivulet are changed according to the cable height.

2.1. Theoretical formulation

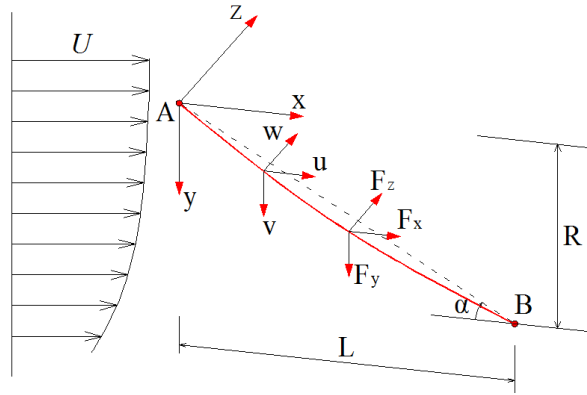


Figure 1. Model of 3 - D continuous cable

Fig. 1 is a schematic diagram of a 3D continuous cable under RWIV. The equations governing the motions of a 3D continuous cable in the in-plane motion can be written as

$$\frac{\partial}{\partial s} \left[(T + \Delta T) \left(\frac{dx}{ds} + \frac{\partial u}{\partial s} \right) \right] + F_x(y, t) = m \frac{\partial^2 u}{\partial t^2} + c \frac{\partial u}{\partial t} \quad (1a)$$

$$\frac{\partial}{\partial s} \left[(T + \Delta T) \left(\frac{dy}{ds} + \frac{\partial v}{\partial s} \right) \right] + F_y(y, t) = m \frac{\partial^2 v}{\partial t^2} + c \frac{\partial v}{\partial t} - mg \quad (1b)$$

where u and v are the longitudinal and vertical components of the in-plane motion, respectively; T and ΔT are the tension and additional tension generated, respectively; m and c are the mass per unit length and damping coefficient of the cable, respectively; $F_x(y, t)$ and $F_y(y, t)$ are wind pressure on the cable according to the x and y axes, respectively; and g is the gravitational acceleration.

In Fig. 2, vertical and horizontal equilibriums of the isolated element of the cable located at (x, y) require that

$$\frac{d}{ds} \left(T \frac{dy}{ds} \right) = -mg \quad (2a)$$

$$T \frac{dx}{ds} = H \quad (2b)$$

$$\Delta H = \Delta T \frac{dx}{ds} \quad (2c)$$

$$\frac{\partial}{\partial s} = \frac{1}{\sqrt{1 + y_x^2}} \frac{\partial}{\partial x} \tag{2d}$$

$$V + \Delta V = \frac{\partial (M + \Delta M)}{\partial s} \approx -EI \left(\frac{d^3 y}{ds^3} + \frac{d^3 v}{ds^3} \right) \approx -EI \frac{d^3 v}{ds^3} \tag{2e}$$

where H and ΔH are the horizontal components of cable tension and additional tension, respectively; V and ΔV are the vertical components of cable tension and additional tension, respectively; y_x is the first derivative of the cable equation at the initial position. In Eq. (2e), $\frac{d^3 y}{ds^3}$ is eliminated owing to the assumption of the cable shape function as a quadratic equation of the horizontal coordinate (presented later).

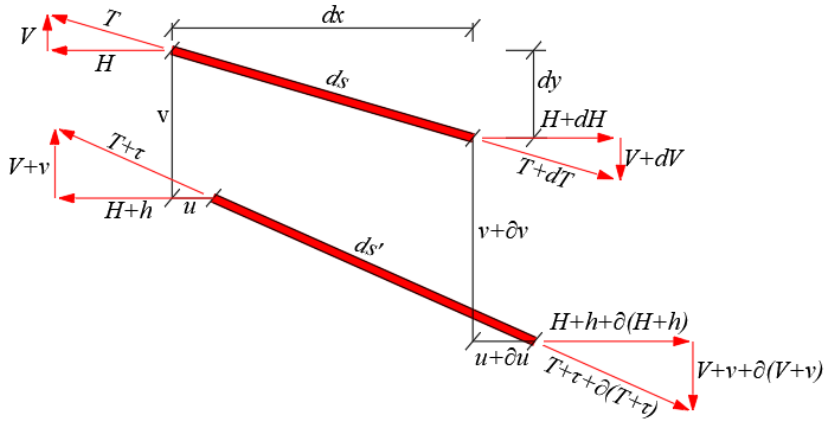


Figure 2. Equilibrium of a cable element

Substituting Eq. (2) into Eq. (1) and neglecting the terms of the second order, the equations of motion are written as follows:

$$\frac{1}{\sqrt{1 + y_x^2}} \frac{\partial}{\partial x} \left[(H + \Delta H) \left(1 + \frac{\partial u}{\partial x} \right) \right] + F_x(y, t) = m \frac{\partial^2 u}{\partial t^2} + c \frac{\partial u}{\partial t} \tag{3a}$$

$$\frac{1}{\sqrt{1 + y_x^2}} \frac{\partial}{\partial x} \left[(H + \Delta H) \left(1 + \frac{\partial v}{\partial x} \right) + \Delta H y_x \right] + F_y(y, t) = m \frac{\partial^2 v}{\partial t^2} + c \frac{\partial v}{\partial t} \tag{3b}$$

Besides that, by applying Hooke's law and neglecting the second order, we have:

$$\frac{\Delta H \left(\frac{ds}{dx} \right)^3}{EA} = \frac{du}{dx} + \frac{dy}{dx} \frac{dv}{dx} \tag{4}$$

where E and A are the elastic modulus and cross-sectional area of cable, respectively.

Substituting Eq. (2d) into Eq. (4), we obtain:

$$\Delta H = \frac{EA}{(1 + y_x^2)^{3/2}} \left(\frac{\partial u}{\partial x} + y_x \frac{\partial v}{\partial x} \right) \tag{5}$$

Substituting Eq. (5) into Eq. (3), the motion of the cable can be written as

$$a_1 \frac{\partial^2 u}{\partial x^2} + a_2 \frac{\partial^2 v}{\partial x^2} + a_3 \frac{\partial u}{\partial x} + a_4 \frac{\partial v}{\partial x} + F_x(y, t) = m \frac{\partial^2 u}{\partial t^2} + c \frac{\partial u}{\partial t} \quad (6a)$$

$$a_5 \frac{\partial^2 v}{\partial x^2} + a_2 \frac{\partial^2 u}{\partial x^2} + a_6 \frac{\partial v}{\partial x} + a_4 \frac{\partial u}{\partial x} + F_y(y, t) = m \frac{\partial^2 v}{\partial t^2} + c \frac{\partial v}{\partial t} \quad (6b)$$

where $a_1, a_2, a_3, a_4, a_5,$ and a_6 are given in Appendix A.

2.2. Discretization of differential equations

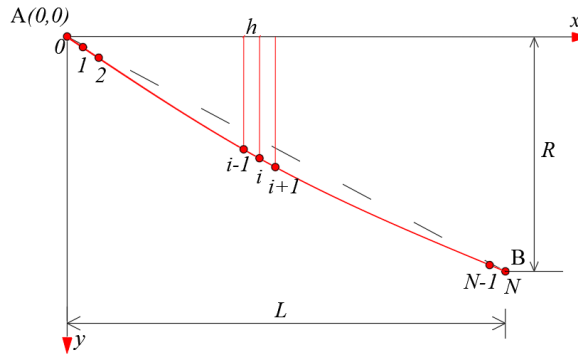


Figure 3. Model of dividing nodes on the cable

To solve Eqs. (6a) and (6b), the cable will be divided into N parts so that the horizontal length of one part is l_h with $l_h = L/N$ as presented in Fig. 3. Using the central difference algorithm for points i from 2 to $N - 2$, the components $\frac{\partial^2 u}{\partial x^2}$ and $\frac{\partial^2 v}{\partial x^2}$ are estimated as

$$\frac{\partial^2 u(x_i)}{\partial x^2} = \frac{1}{l_h^2} (u_{i-1} - 2u_i + u_{i+1}), \quad (7a)$$

$$\frac{\partial^2 v}{\partial x^2} = \frac{1}{l_h^2} (v_{i-1} - 2v_i + v_{i+1}). \quad (7b)$$

At point 1 and point $N - 1$, $\frac{\partial^2 u}{\partial x^2}$ and $\frac{\partial^2 v}{\partial x^2}$ are calculated as follows:

$$\frac{\partial^2 u(x_1)}{\partial x^2} = \frac{1}{l_h^2} (-2u_1 + u_2), \quad \frac{\partial^2 v(x_1)}{\partial x^2} = \frac{1}{l_h^2} (-2v_1 + v_2), \quad (8)$$

$$\frac{\partial^2 u(x_{n-1})}{\partial x^2} = \frac{1}{l_h^2} (u_{n-2} - 2u_{n-1}) \quad \frac{\partial^2 v(x_{n-1})}{\partial x^2} = \frac{1}{l_h^2} (v_{n-2} - 2v_{n-1})$$

The initial conditions are:

$$u_0 = v_0 = u_N = v_N = 0 \quad (9)$$

Substituting Eqs. (8) and (9) into Eq. (7), the discrete equations of motion can be written as follows:

$$[M] \frac{d^2 \{u\}}{dt^2} + [C] \frac{d \{u\}}{dt} + [K] \{u\} = \{F\} \quad (10)$$

where $[K]$, $[M]$, and $[C]$ are the stiffness, mass, and damping matrices, respectively, given in Appendix A; $\{u\}$ is the displacement vector with $\{u\} = [u_1, v_1, \dots, u_i, v_i, \dots, u_{N-1}, v_{N-1}]^T$; and $\{F\}$ is the force vector with $\{F\} = [F_x(y_1, t), F_y(y_1, t), \dots, F_x(y_{N-1}, t), F_y(y_{N-1}, t)]^T$.

The forces $F_x(y_i, t)$ and $F_y(y_i, t)$ can be calculated as

$$F_x(y_i, t) = F_{aerodynamic}(i) \times \sin(\alpha(i)) \quad (11a)$$

$$F_y(y_i, t) = -F_{aerodynamic}(i) \times \cos(\alpha(i)) \quad (11b)$$

where $\alpha(i)$ is the inclination angle at point i and $F_{aerodynamic}(i)$ is the aerodynamic force on the cable per unit length in the localy-axis of the cable cross-section at point i . $F_{aerodynamic}(i)$ is calculated as

$$F_{aerodynamic}(i) = \frac{U_{rel}^2(y_i, t) D \rho}{2} (C_L(\phi_e(i)) \cos(\phi^*(i)) + C_D(\phi_e(i)) \sin(\phi^*(i))) \quad (12)$$

where D is the diameter of the cable; ρ is the density of the air; $U_{rel}(y_i, t)$ is the relative velocity of mean wind to the cable with moving rivulet at point i ; $\phi_e(i)$ is the angle between the relative velocity $U_{rel}(y_i, t)$ and the horizontal axis; C_D , C_L are the drag and lift coefficients, respectively; Angle ϕ_e is computed by the following formula:

$$\phi_e(i) = \phi^*(i) - \theta(i) - \theta_0(i) \quad (13)$$

where $\theta_0(i)$ and $\theta(i)$ are the unstable balance angle and the angle oscillation of the rivulet at point i .

The aerodynamic force $F_{aerodynamic}(i)$ can be calculated by using the following equation proposed by Truong and Vu [24]:

$$F_{aerodynamic}(i) = F_{damp}(i) \cdot \dot{y} + F_{exc}(i) \quad (14)$$

in which y is the vertical direction in the cross-section of the cable; and:

$$F_{damp} = \frac{D\rho}{2} \begin{pmatrix} S_1 + S_2 \sin(\omega t) + S_3 \sin(2\omega t) + S_4 \sin(3\omega t) + S_5 \sin(4\omega t) + \\ S_6 \cos(\omega t) + S_7 \cos(2\omega t) + S_8 \cos(3\omega t) \end{pmatrix} \quad (15)$$

$$F_{exc} = \frac{D\rho}{2} \begin{pmatrix} X_1 + X_2 \sin(\omega t) + X_3 \sin(2\omega t) + X_4 \sin(3\omega t) + X_5 \sin(4\omega t) + \\ X_6 \cos(\omega t) + X_7 \cos(2\omega t) + X_8 \cos(3\omega t) + X_9 \cos(5\omega t) \end{pmatrix} \quad (16)$$

where D and ω are the diameter and frequency of the cable; ρ is the density of the air; and, S_i and X_i are the parameters which can be found in [24]. In summation, the aerodynamic forces acting on the cable element i^{th} are written as

$$F_{damp}(i) = F_{damp}(U(i), \gamma_0(i), \alpha(i), \theta_0(i), a_m(i), t) \quad (17a)$$

$$F_{exc}(i) = F_{exc}(U(i), \gamma_0(i), \alpha(i), \theta_0(i), a_m(i), t) \quad (17b)$$

As can be seen in Eq. (13), aerodynamic forces include two components F_{exc} and F_{damp} , in which F_{damp} continuously changes the damping ratio of oscillation. Thus, the damping matrix $[C]$ and force vector $\{F\}$ in Eq. (10) are rewritten as

$$[DAMP] = [C] + [F_{damp}] \quad (18)$$

$$\{F\} = \{F_{exc}\} \quad (19)$$

where $[F_{damp}]$ and $\{F_{exc}\}$ are given in Appendix A. Now, Eq. (10) is rewritten as

$$[M] \frac{d^2 \{u\}}{dt^2} + [DAMP] \frac{d \{u\}}{dt} + [K] \{u\} = \{F_{exc}\} \quad (20)$$

2.3. Wind velocity function according to height above the ground

As presented in Eqs. (17), the aerodynamic forces acting on the cable element i^{th} are dependent on the wind velocity at the height of point i that is well-known to increase when the height above the ground increases. Wind velocity function according to height above the ground can be calculate as follows:

$$\frac{U_0(y_1, t)}{U_0(y_2, t)} = \left(\frac{y_1}{y_2}\right)^n \quad (21)$$

where $U_0(y_1, t)$ and $U_0(y_2, t)$ are wind velocities at the heights y_1 and y_2 , respectively; n is an empirically derived coefficient that is dependent on the stability of the atmosphere. For neutral stability conditions, n is approximately 1/7, or 0.143. Therefore, n is assumed to be equal to 0.143 in this study.

2.4. Unstable balance angle and aerodynamic forces

Unstable balance angle θ_0 of the rivulet on the cable surface can be found by using the unstable motion of the cable as [29]

$$\Delta = \frac{A}{B} \left[2\zeta + \varepsilon \frac{1}{\pi\mu_r} (C_D(\theta)) + \frac{\partial C_L(\theta, \theta_0)}{\partial \theta} \right] + \varepsilon \frac{1}{\pi\mu_r^2} \frac{\partial C_L(\theta, \theta_0)}{\partial \theta} < 0 \quad (22)$$

where A/B is the amplitude ratio of the cable and rivulet; ζ is the damping ratio of the cable system; $\mu_r = R\omega/U$; $\varepsilon = \pi R^2 \rho/m$.

Notes that, A/B is difficult to precisely predict, thus the criteria for the two limit conditions are assumed as follows:

(a) When $A/B \rightarrow \infty$ or $B \rightarrow 0$, Eq. (22) corresponds to the galloping of the cable. Unstable balance angle can be found from the following equation:

$$2\zeta + \varepsilon \frac{1}{\pi\mu_r} (C_D(\theta)) + \frac{\partial C_L(\theta, \theta_0)}{\partial \theta} < 0 \quad (23)$$

(b) When $A/B \rightarrow 0$, this means that the nondimensional amplitude of the cable is much smaller than that of the rivulet. Eq. (18) is rewritten as follows:

$$\frac{\partial C_L(\theta, \theta_0)}{\partial \theta} < 0 \quad (24)$$

Obviously from Eq. (22), the unstable balance angle θ_0 depends on A/B , so it is difficult to calculate by using numerical analyses. To overcome this problem, in this study the experiment results given in [10] and [16] are used to determine the unstable balance angle θ_0 and the lift and drag coefficients of the cable.

Fig. 4 provided in [23] shows the relationship between the unstable balance angle θ_0 and the amplitude a_m of rivulet according to wind velocity. As presented in this figure, RWIV only occurs when wind velocity is in the range (6.5 m/s, 12.5 m/s). The function of θ_0 and a_m can be fitted from this figure as follows:

$$\theta_0 = 0.0525U_0^3 - 1.75U_0^2 + 14.72U_0 + 24.938 \text{ for } 6.5 < U_0 < 12.5 \text{ (m/s)} \quad (25)$$

$$a_m = -1.9455U_0^4 + 60.543U_0^3 - 699.05U_0^2 + 3557U_0 - 6738.4 \text{ for } 6.5 < U_0 \leq 9.5 \text{ (m/s)} \quad (26a)$$

$$a_m = -2.1667U_0^4 + 97.167U_0^3 - 1626.2U_0^2 + 12028U_0 - 33137 \text{ for } 9.5 < U_0 < 12.5 \text{ (m/s)} \quad (26b)$$

$$a_m = 0 \text{ for } U_0 \leq 6.5 \text{ or } 12.5 \leq U_0 \quad (26c)$$

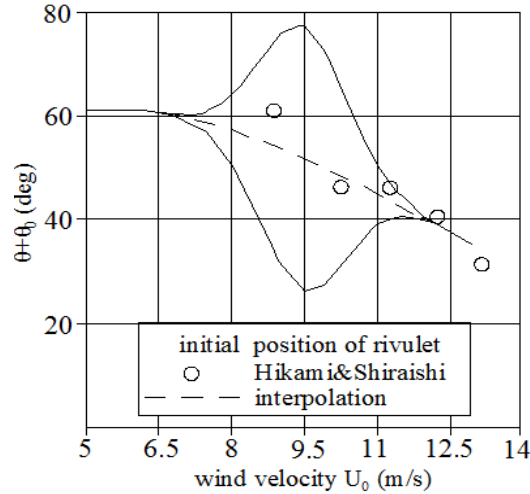


Figure 4. Initial rivulet vs. wind velocity

2.5. Inclination angle of the cable

The function of cable shape is assumed as a quadratic equation of the horizontal coordinate as follows:

$$y = -\frac{mg}{2H} \sec(\alpha) x^2 + \frac{mgL}{2H} \sec(\alpha) x + \tan(\alpha) x \quad (27)$$

The matrix of inclination angle $\{\alpha\}$ has are defined as

$$\tan(\alpha(i)) = \frac{mg}{H} \sec(\alpha) x(i) \quad (28)$$

The matrix of the effective wind speed $\{U\}$ and the wind angle effect $\{\gamma_0\}$ in the cable plane are defined as

$$U(i) = U_0(i) \sqrt{\cos^2 \beta + \sin^2 \alpha(i) \sin^2 \beta} \quad (29)$$

where $\{U_0\}$ is the matrix of initial wind velocity calculated from Eq. (23), and

$$\gamma_0(i) = \sin^{-1} \left(\frac{\sin \alpha(i) \sin \beta}{\sqrt{\cos^2 \beta + \sin^2 \alpha(i) \sin^2 \beta}} \right) \quad (30)$$

2.6. Nonlinear solution procedure

Eq. (20) is a system of second-order differential equations. Among the several numerical methods, the fourth-order method Runge-Kutta appears to be one of the most effective methods for solving nonlinear problems, especially for a system of differential equation. Fig. 5 presents the basic process of a numerical solution for a system of second-order differential equations of the 3D wind-rain induced cable vibration. Firstly, the matrix of initial parameters $\{U_0\}$, $\{\alpha\}$, $\{U\}$, $\{\gamma_0\}$, $\{a_m\}$, and $\{\theta_0\}$ are calculated by using Eqs. (21), (27), (29), (30), (26), and (25), respectively. Secondly, the matrices $[M]$, $[K]$, and $[C]$ are obtained by using Eqs. (A.7), (A.8), and (A.9). Lastly, the fourth-order method Runge-Kutta is used to solve the differential equation of Eq. (20).

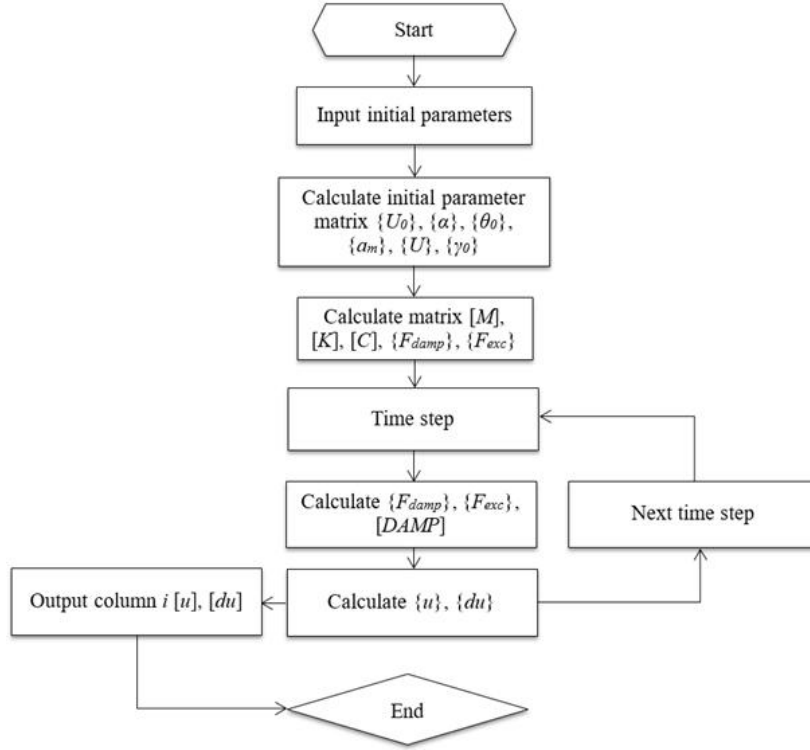


Figure 5. Flowchart of numerical calculation

3. Case studies

In this section, the surveyed cable has the following properties: the length $L_{cab} = 330.4$ m, mass per unit length $m = 81.167$ kg/m, diameter $D = 0.114$ m, first natural frequency $f = 0.42$ Hz, and structural damping ratio $\xi_s = 0.1\%$. RWIV appears in the range of wind velocity from 6.5 m/s to 12.5 m/s, and the maximum amplitude peaks at 9.5 m/s. Eq. (20) is solved with the initial conditions of $y_0 = 0.001$ m and $\dot{y}_0 = 0$. The inclination and the yaw angles are assumed to be 27.8° and 35° , respectively. The drag and lift coefficients C_D and C_L are fitted according to the actual angle between the wind acting on cable and the rivulet, ϕ_e , as the following equation by using Fig. 6 which is given in [20]:

$$C_D = -1.6082\phi_e^3 - 2.4429\phi_e^2 - 0.5065\phi_e + 0.9338 \quad (31a)$$

$$C_L = 1.3532\phi_e^3 + 1.8524\phi_e^2 + 0.1829\phi_e - 0.0073 \quad (31b)$$

To consider the impact of the change of wind velocity, seven cases will be discussed. The first case is that wind velocity is constant and equals 9.5 m/s. The remaining six cases are different wind velocity distributions on the cable corresponding to the different cable heights of 1000 m, 500 m, 300 m, 250 m, 200 m, and 170 m. The range of wind velocities is chosen so that wind velocity at the midpoint of the cable is 9.5 m/s.

Fig. 7 presents the cable responses at $t = 799.7$ (s), showing a maximum cable amplitude at the midpoint. The results are compared with other numerical ones provided in [10] and [28] in Table 1. Note that there are no significant differences between the present results and those of Gu [10] and Li et al. [28], except in the 2D model result. Clearly, the 2D cable model does not consider the cable tension and stiffness, so the results obtained are smaller than those obtained by the 3D model.

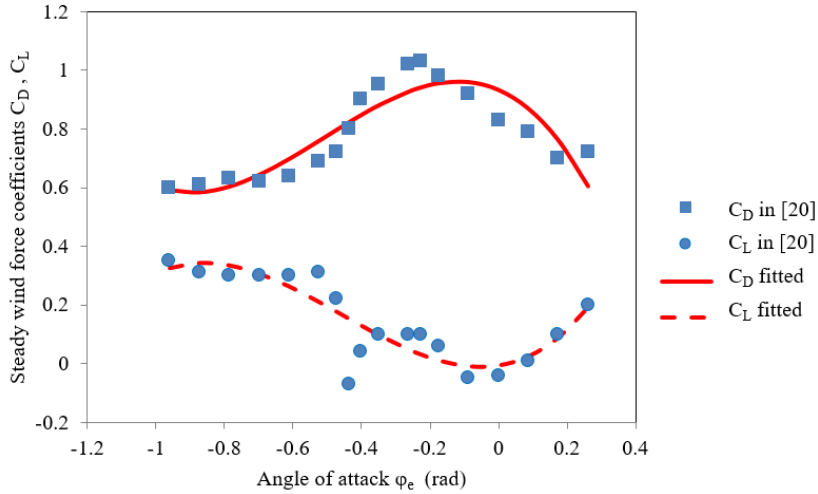


Figure 6. Wind force coefficients for cable with rivulet ($\alpha = 30^\circ, \beta = 35^\circ$)

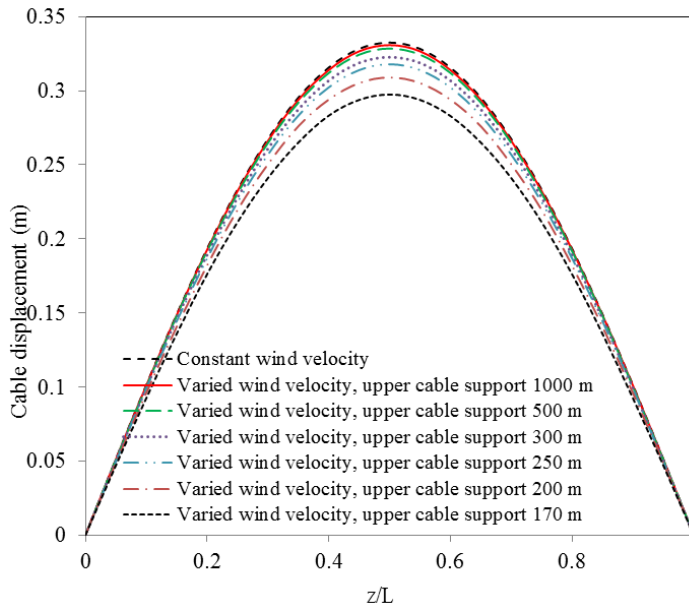


Figure 7. Cable responses with different range of wind speed

Further, the influence of a range of wind velocity on RWIV is obtained. It can be seen in Fig. 7 and Table 1, when the upper cable support is higher, the cable amplitude is larger. When the cable supports are higher than 300 m, the difference of maximum cable amplitudes is not significant (below 3%). When the height of upper cable supports is smaller than 200 m, the difference of maximum cable amplitudes is from 7.08% to 11.64% that cannot be neglected in analysis. According to Gimsing and Georgakis [33], the ratio of the optimum height from the bridge deck to upper cable support to the main span length of a cable-stayed bridge is about 0.17. Since most current cable-stayed bridges have the main span length smaller than 600 m, the distance from the bridge deck to upper cable support is smaller than 100 m, and the height of upper cable support is lower than 200 m. In this case, calculation

of RWIV should include the change of wind velocity according to height above the ground.

Table 1. Comparison of maximum cable displacement responses

	Feature	Range of wind velocity (m/s)	Maximum cable displacement (cm)	Deviation from Gu's result (%)	Deviation from present Case 1 (%)
	Constant wind velocity	9.5	33.26	0.77	-
	Upper cable end: 1000 m	9.38–9.6	33.09	0.26	-0.51
	Upper cable end: 500 m	9.22–9.7	32.85	-0.44	-1.21
Present	Upper cable end: 300 m	8.92–9.85	32.27	-2.20	-2.96
	Upper cable end: 250 m	8.71–9.925	31.79	-3.66	-4.40
	Upper cable end: 200 m	8.26–10.06	30.90	-6.36	-7.08
	Upper cable end: 170 m	7.64–10.322	29.39	-10.95	-11.64
Present	2-D model	9.5	25.80	-21.82	-22.42
Gu, [9]	Varied wind velocity	6.9–8.3	33	-	-0.77
Li, [29]	Constant wind velocity	11	28	-15.15	-15.80

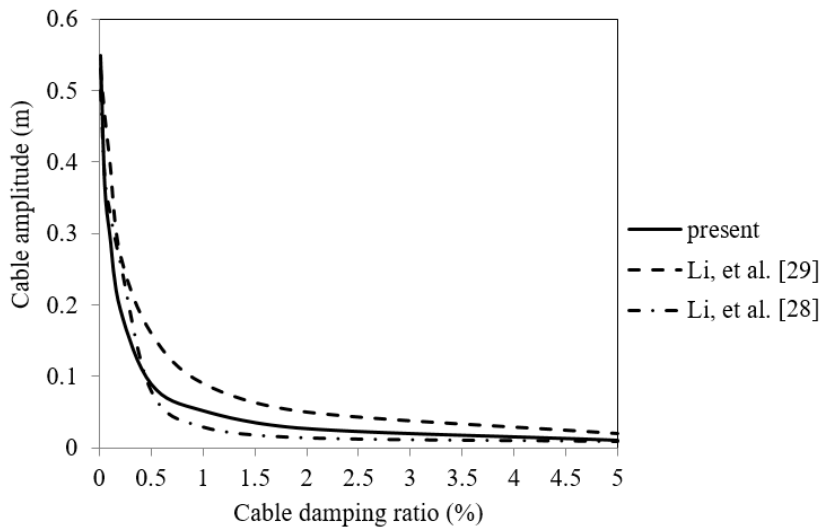


Figure 8. Cable amplitude according to cable damping ratio

Next, the cable with varied wind velocity according to height is discussed with different cable damping ratios. The cable damping ratio changes from 0.01% to 5%, and the results are compared with those of Li et al. [28, 29]. Fig. 8 shows the relationship between maximum cable amplitude and cable damping ratio. Clearly, cable amplitude increases when the cable damping ratio decreases and vice versa. However, when the cable damping ratio is greater than 0.5% the cable amplitude reduces slowly, and when the cable damping ratio is smaller than 0.5% it increases rapidly. These results are similar to those of Li et al. [28, 29].

4. Conclusions

The following points can be summarized from the present study:

- A 3D model for analysis of RWIV of inclined cables using the linear theory of cable vibration and the central difference algorithm is successfully developed that can consider the change of wind speed according to height above the ground.

- When the height of upper cable supports is smaller than 200 m, the difference of maximum cable amplitudes between the RWIV models considering and not considering the change of wind velocity according to height above the ground is from 7.08% to 11.64%. Most current cable-stayed bridges have the main span length smaller than 600m, so the height of their upper cable supports is lower than 200 m. Therefore, calculation of RWIV should include the change of wind velocity according to height above the ground.

- When the height of upper cable support is above 300 m, the effect of wind velocity change according to height can be neglected since the difference of maximum cable amplitudes between the RWIV models considering and not considering the change of wind velocity according to height above the ground is smaller than 3%.

- The amplitude of cable RWIV reduces slowly when the cable damping ratio is higher than 0.5%, but it increases rapidly when the cable damping ratio is lower than 0.5%.

References

- [1] Núñez, G. J. Z., Loredó-Souza, A. M., Rocha, M. M., Bagatini-Cachuço, F. (2018). [Aerodynamic behavior of a cable-stayed bridge section composed by inclined parallel decks](#). *Journal of Wind Engineering and Industrial Aerodynamics*, 173:156–170.
- [2] Demartino, C., Ricciardelli, F. (2015). [Aerodynamic stability of ice-accreted bridge cables](#). *Journal of Fluids and Structures*, 52:81–100.
- [3] Ma, C.-m., Duan, Q.-s., Liao, H.-l. (2018). [Experimental Investigation on Aerodynamic Behavior of a Long Span Cable-stayed Bridge Under Construction](#). *KSCE Journal of Civil Engineering*, 22(7):2492–2501.
- [4] Ma, C., Duan, Q., Li, Q., Liao, H., Tao, Q. (2019). [Aerodynamic characteristics of a long-span cable-stayed bridge under construction](#). *Engineering Structures*, 184:232–246.
- [5] Hikami, Y., Shiraishi, N. (1988). [Rain-wind-induced vibrations of cables in cable stayed bridges](#). *Journal of Wind Engineering and Industrial Aerodynamics*, 29:409–418.
- [6] Bosdogianni, A., Olivari, D. (1996). [Wind-and rain-induced oscillations of cables of stayed bridges](#). *Journal of Wind Engineering and Industrial Aerodynamics*, 64(2-3):171–185.
- [7] Matsumoto, M., Shiraishi, N., Shirato, H. (1992). [Rain-wind induced vibration of cables of cable-stayed bridges](#). *Journal of Wind Engineering and Industrial Aerodynamics*, 43(1-3):2011–2022.
- [8] Flamand, O. (1995). [Rain-wind induced vibration of cables](#). *Journal of Wind Engineering and Industrial Aerodynamics*, 57(2-3):353–362.
- [9] Gu, M., Du, X. (2005). [Experimental investigation of rain-wind-induced vibration of cables in cable-stayed bridges and its mitigation](#). *Journal of Wind Engineering and Industrial Aerodynamics*, 93(1): 79–95.
- [10] Gu, M. (2009). [On wind-rain induced vibration of cables of cable-stayed bridges based on quasi-steady assumption](#). *Journal of Wind Engineering and Industrial Aerodynamics*, 97(7-8):381–391.
- [11] Gao, D., Chen, W.-L., Zhang, R.-T., Huang, Y.-W., Li, H. (2019). [Multi-modal vortex-and rain-wind-induced vibrations of an inclined flexible cable](#). *Mechanical Systems and Signal Processing*, 118:245–258.
- [12] Jing, H., Xia, Y., Li, H., Xu, Y., Li, Y. (2015). [Study on the role of rivulet in rain-wind-induced cable vibration through wind tunnel testing](#). *Journal of Fluids and Structures*, 59:316–327.

- [13] Du, X., Gu, M., Chen, S. (2013). [Aerodynamic characteristics of an inclined and yawed circular cylinder with artificial rivulet](#). *Journal of Fluids and Structures*, 43:64–82.
- [14] Jing, H., Xia, Y., Li, H., Xu, Y., Li, Y. (2017). [Excitation mechanism of rain–wind induced cable vibration in a wind tunnel](#). *Journal of Fluids and Structures*, 68:32–47.
- [15] Wu, T., Kareem, A., Li, S. (2013). [On the excitation mechanisms of rain–wind induced vibration of cables: Unsteady and hysteretic nonlinear features](#). *Journal of Wind Engineering and Industrial Aerodynamics*, 122:83–95.
- [16] Cosentino, N., Flamand, O., Ceccoli, C. (2003). [Rain-wind induced vibration of inclined stay cables-Part I: Experimental investigation and physical explanation](#). *Wind and Structures*, 6(6):471–484.
- [17] Macdonald, J. H. G., Larose, G. L. (2008). [Two-degree-of-freedom inclined cable galloping-Part 2: Analysis and prevention for arbitrary frequency ratio](#). *Journal of wind Engineering and industrial Aerodynamics*, 96(3):308–326.
- [18] Flamand, O., Boujard, O. (2009). A comparison between dry cylinder galloping and rain-wind induced excitation. In *Proceeding of the 5th European & African Conference on Wind Engineering, Florence*.
- [19] Zuo, D., Jones, N. P. (2010). [Interpretation of field observations of wind-and rain-wind-induced stay cable vibrations](#). *Journal of Wind Engineering and Industrial Aerodynamics*, 98(2):73–87.
- [20] Du, X., Gu, M., Chen, S. (2013). [Aerodynamic characteristics of an inclined and yawed circular cylinder with artificial rivulet](#). *Journal of Fluids and Structures*, 43:64–82.
- [21] Yamaguchi, H. (1990). [Analytical study on growth mechanism of rain vibration of cables](#). *Journal of Wind Engineering and Industrial Aerodynamics*, 33(1-2):73–80.
- [22] Xu, Y., Wang, L. (2003). [Analytical study of wind–rain-induced cable vibration: SDOF model](#). *Journal of Wind Engineering and Industrial Aerodynamics*, 91(1-2):27–40.
- [23] Wilde, K., Witkowski, W. (2003). [Simple model of rain-wind-induced vibrations of stayed cables](#). *Journal of Wind Engineering and Industrial Aerodynamics*, 91(7):873–891.
- [24] Hung, T. V., Viet, V. Q. (2019). [A 2D model for analysis of rain-wind induced vibration of stay cables](#). *Journal of Science and Technology in Civil Engineering (STCE)-NUCE*, 13(2):33–47.
- [25] Lemaitre, C., Hémon, P., de Langre, E. (2007). [Thin water film around a cable subject to wind](#). *Journal of Wind Engineering and Industrial Aerodynamics*, 95(9-11):1259–1271.
- [26] Bi, J. H., Wang, J., Shao, Q., Lu, P., Guan, J., Li, Q. B. (2013). [2D numerical analysis on evolution of water film and cable vibration response subject to wind and rain](#). *Journal of Wind Engineering and Industrial Aerodynamics*, 121:49–59.
- [27] Jing, H., He, X., Wang, Z. (2018). [Numerical modeling of the wind load of a two-dimensional cable model in rain–wind-induced vibration](#). *Journal of Fluids and Structures*, 82:121–133.
- [28] Li, S. Y., Gu, M., Chen, Z. Q. (2007). Analytical model for rain–wind-induced vibration of three-dimensional continuous stay cable with quasi-moving rivulet. *Engineering Mechanics*, 24(6):7–12.
- [29] Li, S. Y., Gu, M., Chen, Z. Q. (2009). An analytical model for rain-wind-induced vibration of three-dimensional continuous stay cable with actual moving rivulet. *Journal of Human University (natural Sciences)*, 36:1–7.
- [30] Li, S. Y., Wu, T., Li, S. K., Gu, M. (2016). [Numerical study on the mitigation of rain-wind induced vibrations of stay cables with dampers](#). *Wind and Structures*, 23(6):615–639.
- [31] Liu, X., Huo, B., Zhang, S. (2013). [Nonlinear dynamic analysis on the rain-wind-induced vibration of cable considering the equilibrium position of rivulet](#). *Advances in Civil Engineering*, 2013.
- [32] Irvine, H. M. (1981). *Cable structure*. The MIT Press, Cambridge, Massachusetts, and London, England.
- [33] Gimsing, N. J., Georgakis, C. T. (2012). *Cable supported bridges*. John Wiley & Sons Ltd, United Kingdom.

Appendix A.

$$a_1 = \frac{H}{\sqrt{1 + y_x^2}} + \frac{EA}{(1 + y_x^2)^2} \quad (\text{A.1})$$

